

## Radiative neutralino production in low energy supersymmetric models

Rahul Basu,<sup>1,\*</sup> P. N. Pandita,<sup>2,3,+</sup> and Chandradew Sharma<sup>1,‡</sup>

<sup>1</sup>*The Institute of Mathematical Sciences, Chennai 600 113, India*

<sup>2</sup>*Department of Physics, North Eastern Hill University, Shillong 793 022, India*<sup>§</sup>

<sup>3</sup>*The Abdus Salam International Centre for Theoretical Physics, Strada Costiera 11, 34014 Trieste, Italy*  
(Received 15 November 2007; revised manuscript received 7 March 2008; published 13 June 2008)

We study the production of the lightest neutralinos in the radiative process  $e^+e^- \rightarrow \tilde{\chi}_1^0\tilde{\chi}_1^0\gamma$  in low energy supersymmetric models for the International Linear Collider energies. This includes the minimal supersymmetric standard model as well as its extension with an additional chiral Higgs singlet superfield, the nonminimal supersymmetric standard model. We compare and contrast the dependence of the signal cross section on the parameters of the neutralino sector of the minimal and nonminimal supersymmetric standard model. We also consider the background to this process coming from the standard model process  $e^+e^- \rightarrow \nu\bar{\nu}\gamma$ , as well as from the radiative production of the scalar partners of the neutrinos (sneutrinos)  $e^+e^- \rightarrow \tilde{\nu}\tilde{\nu}^*\gamma$ , which can be a background to the radiative neutralino production when the sneutrinos decay invisibly. In low energy supersymmetric models radiative production of the lightest neutralinos may be the only channel to study supersymmetric partners of the standard model particles at the first stage of a linear collider, since heavier neutralinos, charginos, and sleptons may be too heavy to be pair produced at a  $e^+e^-$  machine with  $\sqrt{s} = 500$  GeV.

DOI: [10.1103/PhysRevD.77.115009](https://doi.org/10.1103/PhysRevD.77.115009)

PACS numbers: 11.30.Pb, 12.60.Jv, 14.80.Ly

### I. INTRODUCTION

Supersymmetry (SUSY) is, at present, the only known framework [1] in which the Higgs sector of the standard model (SM), so essential for its internal consistency, is technically natural [2]. Supersymmetry is, however, not an exact symmetry in nature. The precise manner in which SUSY is broken is not known at present. However, the necessary SUSY breaking can be introduced through soft supersymmetry breaking terms that do not reintroduce quadratic divergences in the Higgs mass, and thereby do not disturb the stability of the hierarchy between the weak scale and the large grand unified (GUT) scale. Such terms can typically arise in supergravity theories, in which local supersymmetry is spontaneously broken in a hidden sector, and is then transmitted to the visible sector via gravitational interactions. A particularly attractive implementation of the idea of supersymmetry, with soft supersymmetry breaking terms generated by supergravity, is the minimal supersymmetric standard model (MSSM) obtained by simply introducing the supersymmetric partners of the SM states, and introducing an additional Higgs doublet, with opposite hypercharge to that of the SM Higgs doublet, in order to cancel the gauge anomalies and generate masses for all the fermions of the standard model [3,4]. In order for broken supersymmetry to be effective in protecting the weak scale against large radiative corrections, the supersymmetric partners of the SM

particles should have masses of the order of a few hundred GeV. Their discovery is one of the main goals of present and future accelerators. In particular, a  $e^+e^-$  linear collider with a high luminosity  $\mathcal{L} = 500 \text{ fb}^{-1}$ , and a center-of-mass energy of  $\sqrt{s} = 500$  GeV in the first stage, will be an important tool in determining the parameters of the low energy supersymmetric model with a high precision [5–9]. Furthermore, polarization of the electron (and positron) beam can enhance the capability of such a linear collider [10] in unraveling the structure of the underlying supersymmetric model.

In the minimal supersymmetric standard model the fermionic partners of the two Higgs doublets ( $H_1, H_2$ ) mix with the fermionic partners of the gauge bosons to produce four neutralino states  $\tilde{\chi}_i^0$ ,  $i = 1, 2, 3, 4$ , and two chargino states  $\tilde{\chi}_j^\pm$ ,  $j = 1, 2$ . In the MSSM with  $R$ -parity ( $R_p$ ) conservation, the lightest neutralino state is expected to be the lightest supersymmetric particle (LSP). The neutralino states of the minimal supersymmetric standard model with  $R_p$  conservation have been studied in great detail, because the lightest neutralino, being the LSP, is the end product of any process involving supersymmetric particles in the final state.

However, the MSSM suffers from the so-called  $\mu$  problem associated with the bilinear term connecting the two Higgs doublet superfields  $H_1$  and  $H_2$  in the superpotential. An elegant solution to this problem is to postulate the existence of a chiral electroweak gauge singlet superfield  $S$ , and couple it to the two Higgs doublet superfields  $H_1$  and  $H_2$  via a dimensionless trilinear term  $\lambda H_1 H_2 S$  in the superpotential. When the scalar component of the singlet superfield  $S$  obtains a vacuum expectation value, a bilinear term  $\lambda H_1 H_2 \langle S \rangle$  involving the two Higgs doublets is natu-

\*rahul@imsc.res.in

+ppandita@nehu.ac.in

‡sharma@imsc.res.in

§Permanent address.

rally generated. Furthermore, when this scalar component of the chiral singlet superfield  $S$  acquires a vacuum expectation value of the order of the  $SU(2)_L \times U(1)_Y$  breaking scale, it gives rise to an effective value of  $\mu$  ( $\mu_{\text{eff}} \equiv \lambda\langle S \rangle = \lambda x$ ) of the order of the electroweak scale. However, the inclusion of the singlet superfield leads to an additional trilinear superpotential coupling  $(\kappa/3)S^3$  in the model, the so-called nonminimal, or next-to-minimal [11–17], supersymmetric standard model (NMSSM). The absence of the  $H_1 H_2$  term, and the absence of tadpole and mass couplings,  $S$  and  $S^2$ , in the NMSSM, is made natural by postulating a suitable discrete symmetry [18,19]. The NMSSM is attractive on account of the simple resolution it offers to the  $\mu$  problem, and of the scale invariance of its classical action in the supersymmetric limit. Since no dimensional supersymmetric parameters are present in the superpotential of the NMSSM, it is the simplest supersymmetric extension of the standard model in which the electroweak scale originates from the supersymmetry breaking scale only. Its enlarged Higgs sector may help in relaxing the fine-tuning and little hierarchy problems of the MSSM [20], thereby opening new perspectives for the Higgs boson searches at high energy colliders [21,22], and for dark matter searches [23]. In the nonminimal supersymmetric standard model the mixing of fermionic partners of Higgs and gauge bosons [24–26] produces five neutralino states,  $\tilde{\chi}_i^0$ ,  $i = 1, 2, 3, 4, 5$ , and two chargino states,  $\tilde{\chi}_j^\pm$ ,  $j = 1, 2$ . Furthermore, because of the presence of the fermionic partner of the singlet Higgs boson, the neutralino states can have an admixture of this  $SU(2)_L \times U(1)_Y$  singlet fermion, thereby affecting the phenomenology of the neutralinos in the nonminimal supersymmetric standard model.

The lightest neutralino state ( $\tilde{\chi}_1^0$ ) of the MSSM or NMSSM, being typically the LSP, is stable and therefore a possible dark matter candidate [27,28]. Since the neutralinos are among the lightest particles in low energy supersymmetric models, they are expected to be the first states to be produced at the colliding beam experiments. At an electron-positron collider, such as the International Linear Collider (ILC), they can be directly produced in pairs,

$$e^+ + e^- \rightarrow \tilde{\chi}_i^0 + \tilde{\chi}_j^0, \quad (1.1)$$

which proceeds via  $Z$  boson and selectron exchange [29,30]. In collider experiments the LSP escapes detection such that the direct production of the lightest neutralino pair,

$$e^+ + e^- \rightarrow \tilde{\chi}_1^0 + \tilde{\chi}_1^0, \quad (1.2)$$

is invisible. Therefore, one must look for the signature of neutralinos in the radiative process

$$e^+ + e^- \rightarrow \tilde{\chi}_1^0 + \tilde{\chi}_1^0 + \gamma \quad (1.3)$$

where the final photon is radiated off of the incoming

beams or the exchanged selectrons. We note that this process is suppressed by the square of the electromagnetic coupling. However, it might be the first process in which the lightest supersymmetric states could be observed at colliders. The signal of the radiative process (1.3) is a single high energy photon with the missing energy carried away by the neutralinos. The process (1.3) has been studied in detail in the minimal supersymmetric model [31–41]. In these studies, different approximations have been used in calculating the cross section for (1.3), and the focus has been on CERN LEP energies and special neutralino mixing, especially the case where the neutralino is a pure photino [31–38].

More recently, calculations have been carried out in the context of the MSSM assuming general neutralino mixing [39–41]. Some of these studies underline the importance of longitudinal [39] and even transverse beam polarizations. On the other hand, the signature “photon plus missing energy” has been studied in detail by different LEP collaborations, including ALEPH [42], DELPHI [43], L3 [44], and OPAL [45,46]. We recall that in the SM, the radiative neutralino process  $e^+ e^- \rightarrow \nu \bar{\nu} \gamma$  is the leading process with this signature, for which the cross section depends on the number  $N_\nu$  of light neutrino species [47]. This signature has, thus, been used to measure  $N_\nu$ , which has been found to be consistent with 3. Furthermore, the LEP collaborations have found no deviations from the SM prediction, and, therefore, only bounds on the masses of supersymmetric particles have been set [42–44,46]. This process is also important in determining collider bounds on a very light neutralino [48]. For a review of the experimental situation, see Ref. [49].

Most of the theoretical studies on radiative neutralino production in the literature have been carried out in the framework of the minimal supersymmetric standard model. This includes calculations relevant to ILC with a high center-of-mass energy, high luminosity, and longitudinally polarized beams, as well as the study of the SM background from the radiative neutrino production

$$e^+ e^- \rightarrow \nu + \bar{\nu} + \gamma, \quad (1.4)$$

and the MSSM background from radiative sneutrino production

$$e^+ e^- \rightarrow \tilde{\nu} + \tilde{\nu}^* + \gamma. \quad (1.5)$$

It has been pointed out [50] that the discovery potential of the ILC might be significantly extended if both beams are polarized, especially if other SUSY states like heavier neutralino, chargino, or even slepton pairs are too heavy to be produced at the first stage of the ILC at  $\sqrt{s} = 500$  GeV.

In this paper we shall consider the radiative process (1.3) in the nonminimal supersymmetric standard model. As discussed above, the nonminimal supersymmetric standard model is an attractive alternative to the MSSM, which

solves the  $\mu$  problem of the minimal supersymmetric standard model, and in which the weak scale originates from the supersymmetry breaking scale only. Furthermore, the NMSSM has five neutralino states in its spectrum, and there is an admixture of a singlet state in the neutralino states, which may affect the radiative neutralino production process (1.3). On the other hand, the background processes from the SM and supersymmetry are not affected by the spectrum of neutralino states. We shall compare and contrast the signal for the radiative neutralino process in the NMSSM with that in the MSSM, and study in detail the dependence of the cross sections on the parameters of the neutralino sector.

The plan of the paper is as follows. In Sec. II we discuss the cross section for the signal process (1.3) in the NMSSM, and compare and contrast it with the corresponding cross section in the MSSM. Here we recall the basic features of the neutralino mixing matrix in the NMSSM and MSSM, and the couplings of the neutralinos relevant for our calculations, as well as the cross section and the phase space for the signal process. Here we also describe the cuts on the photon angle and energy that are used to regularize the infrared and collinear divergences in the tree-level cross section. We then describe the typical set of input parameters for the NMSSM that are used in our numerical evaluation of the cross sections. The set of parameters that we use are obtained by imposing various experimental and theoretical constraints on the parameter space of the NMSSM. On the other hand, for the MSSM we use the typical benchmark parameter set of the Snowmass Points and Slopes 1a (SPS 1a) scenario [51], except when otherwise indicated. We analyze numerically the dependence of the cross section on the parameters of the neutralino sector, and on the selectron masses. In Sec. III we

discuss the backgrounds to the radiative neutralino production process (1.3) from the SM and supersymmetric processes. Here we also define a statistical significance for measuring an excess of photons from radiative neutralino production over the backgrounds. We summarize our results and conclusions in Sec. IV.

## II. RADIATIVE NEUTRALINO PRODUCTION

### A. Neutralino mass matrix, Lagrangian, and couplings

In order to calculate the cross section for the radiative production of neutralinos,

$$e^-(p_1) + e^+(p_2) \rightarrow \tilde{\chi}_1^0(k_1) + \tilde{\chi}_1^0(k_2) + \gamma(q), \quad (2.1)$$

where the symbols in the brackets denote the four momenta of the respective particles, we need to compute the couplings of the neutralinos to electrons and the scalar partners of electrons, the selectrons. These can be obtained from the neutralino mixing matrix. To obtain the neutralino mixing matrix for the MSSM, we recall that the neutralino mass matrix obtains contributions from part of the MSSM superpotential,

$$W_{\text{MSSM}} = \mu H_1 H_2, \quad (2.2)$$

where  $H_1$  and  $H_2$  are the two Higgs doublet chiral superfields, and  $\mu$  is the supersymmetric Higgs(ino) parameter. In addition to the contribution from the superpotential, the neutralino mass matrix receives contributions from the interactions between gauge and matter multiplets, as well as contributions from the soft supersymmetry breaking masses for the gauginos. Including all these contributions, the neutralino mass matrix, in the  $b$ -ino,  $W$ -ino, Higgsino basis  $(-i\lambda', -i\lambda^3, \psi_{H_1}^1, \psi_{H_2}^2)$ , can be written as [52,53]

$$M_{\text{MSSM}} = \begin{pmatrix} M_1 & 0 & -m_Z \sin\theta_w \cos\beta & m_Z \sin\theta_w \sin\beta \\ 0 & M_2 & m_Z \cos\theta_w \cos\beta & -m_Z \cos\theta_w \sin\beta \\ -m_Z \sin\theta_w \cos\beta & m_Z \cos\theta_w \cos\beta & 0 & -\mu \\ m_Z \sin\theta_w \sin\beta & -m_Z \cos\theta_w \sin\beta & -\mu & 0 \end{pmatrix}, \quad (2.3)$$

where  $M_1$  and  $M_2$  are the  $U(1)_Y$  and the  $SU(2)_L$  soft supersymmetry breaking gaugino mass parameters, respectively, and  $\tan\beta = v_2/v_1$  is the ratio of the vacuum expectation values of the neutral components of the two Higgs doublet fields  $H_1$  and  $H_2$ , respectively. Furthermore,  $m_Z$  is the  $Z$  boson mass, and  $\theta_w$  is the weak mixing angle. In the  $CP$  conserving case,  $M$  is a real symmetric matrix and can be diagonalized by an orthogonal matrix. Since at least one eigenvalue of  $M$  is negative, we can use a unitary matrix  $N$ , the neutralino mixing matrix, to get a positive semidefinite diagonal matrix [52] with the neutralino masses  $m_{\chi_i^0}$ :

$$N^* M_{\text{MSSM}} N^{-1} = \text{diag}(m_{\chi_1^0}, m_{\chi_2^0}, m_{\chi_3^0}, m_{\chi_4^0}). \quad (2.4)$$

We note that the transformation Eq. (2.4) is only a similarity transformation if  $N$  is real.

For the NMSSM, the relevant part of the superpotential is

$$W_{\text{NMSSM}} = \lambda S H_1 H_2 - \frac{\kappa}{3} S^3, \quad (2.5)$$

where  $S$  is the Higgs singlet chiral superfield. In the basis  $(-i\lambda', -i\lambda^3, \psi_{H_1}^1, \psi_{H_2}^2, \psi_S)$ , the neutralino mass matrix for the NMSSM can then be written as [24,25]

$$M_{\text{NMSSM}} = \begin{pmatrix} M_1 & 0 & -m_Z \sin\theta_w \cos\beta & m_Z \sin\theta_w \sin\beta & 0 \\ 0 & M_2 & m_Z \cos\theta_w \cos\beta & -m_Z \cos\theta_w \sin\beta & 0 \\ -m_Z \sin\theta_w \cos\beta & m_Z \cos\theta_w \cos\beta & 0 & -\lambda x & -\lambda v_2 \\ m_Z \sin\theta_w \sin\beta & -m_Z \cos\theta_w \sin\beta & -\lambda x & 0 & -\lambda v_1 \\ 0 & 0 & -\lambda v_2 & -\lambda v_1 & 2\kappa x \end{pmatrix}, \quad (2.6)$$

where  $\langle S \rangle = x$  is the vacuum expectation value of the singlet Higgs field. As in the case of the MSSM, we can use a unitary matrix  $N'$  to get a positive semidefinite diagonal matrix with the neutralino masses  $m_{\chi_i^0}$  [24,25]:

$$N'^* M_{\text{NMSSM}} N'^{-1} = \text{diag}(m_{\chi_1^0}, m_{\chi_2^0}, m_{\chi_3^0}, m_{\chi_4^0}, m_{\chi_5^0}). \quad (2.7)$$

The Lagrangian for the interaction of neutralinos, electrons, selectrons, and  $Z$  bosons for the MSSM is given by [52]

$$\begin{aligned} \mathcal{L} = & \left( -\frac{\sqrt{2}e}{\cos\theta_w} N_{11}^* \right) \bar{f}_e P_L \tilde{\chi}_1^0 \tilde{e}_R + \frac{e}{\sqrt{2} \sin\theta_w} \\ & \times (N_{12} + \tan\theta_w N_{11}) \bar{f}_e P_R \tilde{\chi}_1^0 \tilde{e}_L + \frac{e}{4 \sin\theta_w \cos\theta_w} \\ & \times (|N_{13}|^2 - |N_{14}|^2) Z_\mu \bar{\chi}_1^0 \gamma^\mu \gamma^5 \tilde{\chi}_1^0 \\ & + e Z_\mu \bar{f}_e \gamma^\mu \left[ \frac{1}{\sin\theta_w \cos\theta_w} \left( \frac{1}{2} - \sin^2\theta_w \right) P_L \right. \\ & \left. - \tan\theta_w P_R \right] f_e + \text{H.c.}, \end{aligned} \quad (2.8)$$

with the electron, selectron, neutralino, and  $Z$  boson fields denoted by  $f_e$ ,  $\tilde{e}_{L,R}$ ,  $\tilde{\chi}_1^0$ , and  $Z_\mu$ , respectively, and  $P_{R,L} = \frac{1}{2}(1 \pm \gamma^5)$ . The corresponding interaction Lagrangian for the NMSSM is obtained from (2.8) by replacing  $N_{ij}$  with  $N'_{ij}$ . The different vertices following from (2.8) are shown in Table I.

The couplings of the lightest neutralino to electrons, selectrons, and  $Z$  bosons are determined by the corresponding elements of the neutralino mixing matrix ( $N_{ij}$  or  $N'_{ij}$ ). For numerical calculation of the radiative neutralino cross section in the MSSM, we have chosen to work with the parameters in the SPS 1a scenario [51]. The parameters of the SPS 1a scenario are summarized in Table II. However, since in the SPS 1a scenario the values of the parameters  $\mu$  and  $M_2$  are fixed, we shall use a different set of parameters to study the dependence of the neutralino mass and the radiative neutralino production cross section on  $\mu$  and  $M_2$ , and on the selectron masses. This set of parameters is shown in Table III. We shall call this set of parameters the MSSM electroweak symmetry breaking scenario (EWSB) [54].

On the other hand, for the NMSSM we use a set of parameters that is obtained by imposing theoretical and experimental constraints on the parameter space of the NMSSM. The parameters that enter the neutralino mass matrix of the NMSSM are, apart from  $M_1$  and  $M_2$ ,  $\tan\beta$ ,  $\mu$  ( $\equiv \lambda \langle S \rangle = \lambda x$ ),  $\lambda$ , and  $\kappa$ . For  $M_1$ ,  $M_2$ , and  $M_3$ , we use the values which are consistent with the usual GUT relation  $M_1/\alpha_1 = M_2/\alpha_2 = M_3/\alpha_3$ . We note that for the MSSM in SPS 1a scenario, the value of the parameter  $\tan\beta = 10$ . In order to remain close to the SPS 1a scenario of the MSSM, we have chosen for our numerical calculations in the NMSSM  $\tan\beta = 10$ , whereas the rest of the parameters are chosen in such a way that the lightest Higgs boson

TABLE I. Vertices corresponding to various terms in the interaction Lagrangian (2.8) for the MSSM. In addition, we have also shown the vertices for selectron-photon and electron-photon interactions. The vertices for the NMSSM are obtained by replacing  $N_{ij}$  with  $N'_{ij}$ .

Vertex	Vertex factor
Right-selectron–electron–neutralino	$\frac{-ie\sqrt{2}}{\cos\theta_w} N_{11}^* P_L$
Left-selectron–electron–neutralino	$\frac{ie}{\sqrt{2} \sin\theta_w} (N_{12} + \tan\theta_w N_{11}) P_R$
Neutralino– $Z^0$ –neutralino	$\frac{ie}{4 \sin\theta_w \cos\theta_w} ( N_{13} ^2 -  N_{14} ^2) \gamma^\mu \gamma^5$
Electron– $Z^0$ –electron	$ie \gamma^\mu \left[ \frac{1}{\sin\theta_w \cos\theta_w} \left( \frac{1}{2} - \sin^2\theta_w \right) P_L - \tan\theta_w P_R \right]$
Selectron–photon–selectron	$ie(p_1 + p_2)^\mu$
Electron–photon–electron	$ie \gamma^\mu$

TABLE II. Input parameters and resulting masses for various states in the MSSM SPS 1a scenario.

$\tan\beta = 10$	$\mu = 358 \text{ GeV}$	$M_2 = 192 \text{ GeV}$	$m_0 = 100 \text{ GeV}$
$m_{\chi_1^0} = 97 \text{ GeV}$	$m_{\chi_1^\pm} = 180 \text{ GeV}$	$m_{\tilde{e}_R} = 136 \text{ GeV}$	$m_H = 400 \text{ GeV}$
$m_{\chi_2^0} = 181 \text{ GeV}$	$m_{\chi_2^\pm} = 383 \text{ GeV}$	$m_{\tilde{e}_L} = 196 \text{ GeV}$	$m_h = 111 \text{ GeV}$

TABLE III. Input parameters and resulting masses of various states in the MSSM EWSB scenario.

$\tan\beta = 10$	$\mu = 130 \text{ GeV}$	$M_1 = 150 \text{ GeV}$	$M_2 = 300 \text{ GeV}$
$M_3 = 1000 \text{ GeV}$	$A_t = 3000 \text{ GeV}$	$A_b = 3000 \text{ GeV}$	$A_\tau = 1000 \text{ GeV}$
$m_{\chi_1^0} = 97 \text{ GeV}$	$m_{\chi_1^\pm} = 119 \text{ GeV}$	$m_{\tilde{e}_R} = 143 \text{ GeV}$	$m_{\tilde{\nu}_e} = 194 \text{ GeV}$
$m_{\chi_2^0} = -141 \text{ GeV}$	$m_{\chi_2^\pm} = 330 \text{ GeV}$	$m_{\tilde{e}_L} = 204 \text{ GeV}$	$m_h = 120 \text{ GeV}$

TABLE IV. Input parameters and resulting masses of various states in the NMSSM.

$\tan\beta = 10$	$\mu = 130 \text{ GeV}$	$M_1 = 150 \text{ GeV}$	$M_2 = 300 \text{ GeV}$
$M_3 = 1000 \text{ GeV}$	$A_t = 3000 \text{ GeV}$	$A_b = 3000 \text{ GeV}$	$A_\tau = 1000 \text{ GeV}$
$\lambda = 0.55$	$\kappa = 0.44$	$A_\lambda = 880 \text{ GeV}$	$A_\kappa = 10 \text{ GeV}$
$m_{\chi_1^0} = 77 \text{ GeV}$	$m_{\chi_1^\pm} = 121 \text{ GeV}$	$m_{\tilde{e}_R} = 149 \text{ GeV}$	$m_{\tilde{\nu}_e} = 194 \text{ GeV}$
$m_{\chi_2^0} = -158 \text{ GeV}$	$m_{\chi_2^\pm} = 334 \text{ GeV}$	$m_{\tilde{e}_L} = 209 \text{ GeV}$	$m_h = 122 \text{ GeV}$

mass, the lightest neutralino mass, and the lightest chargino mass satisfy the present experimental lower limits. We have also imposed on the parameter space of the NMSSM the theoretical constraint that there is no charge and color breaking global minimum of the scalar potential, and that a Landau pole does not develop below the grand unified scale ( $M_{\text{GUT}} \approx 10^{16} \text{ GeV}$ ). For instance, for the parameter values  $\tan\beta = 10$ ,  $\mu = 130 \text{ GeV}$ ,  $\lambda = 0.55$ , and  $\kappa = 0.44$ , we obtain the lightest Higgs boson mass of about 123 GeV, and the lightest neutralino boson mass of about 77 GeV, both of which are phenomenologically acceptable values. As another example, choosing  $\tan\beta = 10$  and  $\mu = 225 \text{ GeV}$  results in the lightest Higgs boson mass of about 114 GeV, and the lightest neutralino mass of about 132 GeV but with a charge and color breaking global minimum. Other choices give a Landau pole below  $M_{\text{GUT}}$ , etc. for some particular set of free parameters. It is important to note that a choice of parameters away from  $\tan\beta = 10$  is also possible; for example,  $\tan\beta = 3$ ,  $\mu = 180 \text{ GeV}$ ,  $\lambda = 0.3$ , and  $\kappa = 0.1$  produce a lightest Higgs boson mass of about 114 GeV, and a lightest neutralino mass of about 103 GeV. We have taken  $\tan\beta = 10$  for the NMSSM simply because we wish to compare our results with the MSSM for the typical SPS 1a scenario. The consequence of imposing these constraints on the parameter space of the NMSSM, and the resulting masses for various particles for a particular choice of input parameters are summarized in Table IV.

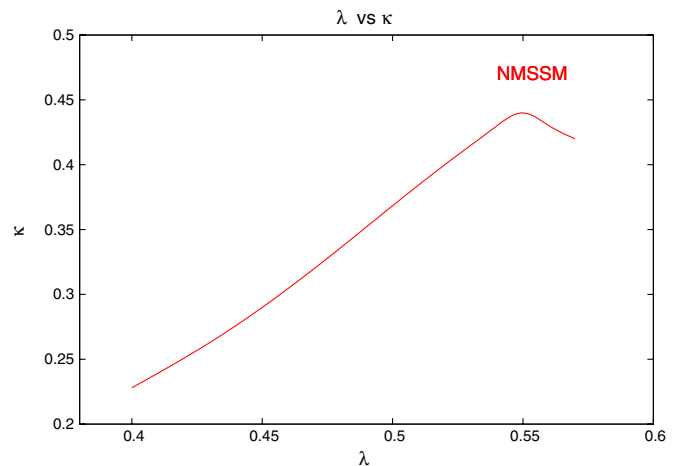
Since the neutralino mass matrix depends on the parameters  $\lambda$  and  $\kappa$ , it is useful to study the possible values of these parameters, with all other parameters fixed, which satisfy the phenomenological and theoretical constraints discussed above. In Fig. 1 we show a plot of  $\lambda$  versus  $\kappa$ , with all other input parameters fixed as in Table IV, and with the lightest neutralino, the lightest Higgs boson, and the lightest chargino mass as in Table IV with a variation of less than 5%. Figure 1 shows the range of  $\lambda$  and  $\kappa$  values that are consistent with all the constraints discussed above for the set of input parameters in Table IV.

We note that for the set of input values in Table IV, values of  $\lambda \lesssim 0.4$ , with  $\kappa \lesssim 0.22$ , lead to an unphysical global minimum. On the other hand, values of  $\lambda \gtrsim 0.57$ , with  $\kappa \gtrsim 0.44$ , lead to a Landau pole below the GUT scale. Thus, the allowed values of  $\lambda$  and  $\kappa$ , for the given set of input parameters, and for the fixed masses of the lightest neutralino, the lightest Higgs boson, and the lightest chargino, as in Table IV, lie in a narrow range  $0.4 \lesssim \lambda \lesssim 0.57$  for  $0.22 \lesssim \kappa \lesssim 0.44$ . For definiteness, we have chosen to work with the values of  $\lambda = 0.55$  and  $\kappa = 0.44$  in this paper. These values correspond to the peak in the  $\lambda$  versus  $\kappa$  plot in Fig. 1.

For the parameters of Table IV, the composition of the lightest neutralino in the NMSSM is given by

$$N'_{1j} = (0.39, -0.22, 0.57, -0.59, 0.35). \quad (2.9)$$

From the composition (2.9), we see that the lightest neutralino has a sizable singlet component, thereby changing the neutralino phenomenology in the NMSSM as compared to the MSSM. For comparison, we also show the


 FIG. 1 (color online). Plot of  $\lambda$  versus  $\kappa$  for the set of input parameters in Table IV.

particle content of the lightest neutralino in the MSSM,

$$N_{1j} = (0.5, -0.21, 0.66, -0.51), \quad (2.10)$$

for the parameter set in Table III. In Fig. 2 we have plotted the constant contour plots for the mass of the lightest neutralino in the NMSSM in the  $\mu$ - $M_2$  plane. We emphasize that the choices of  $\mu$  and  $M_2$  values in this plot have been taken to be consistent with phenomenological and theoretical constraints as described above. For comparison, we have also plotted the corresponding contour plots for the MSSM in Fig. 3 with parameters as in Table III.

### B. Cross section for the signal process

In the NMSSM, and in the MSSM, the process (2.1) proceeds at the tree level via  $t$ - and  $u$ -channel exchange of right and left selectrons  $\tilde{e}_{R,L}$ , and via  $Z$  boson exchange in the  $s$  channel. The corresponding Feynman diagrams are shown in Fig. 4. The differential cross section for (2.1) can be written as [33,55]

$$d\sigma = \frac{1}{2} \frac{(2\pi)^4}{2s} \prod_f \frac{d^3\mathbf{p}_f}{(2\pi)^3 2E_f} \delta^{(4)}(p_1 + p_2 - k_1 - k_2 - q) |\mathcal{M}|^2, \quad (2.11)$$

where  $\mathbf{p}_f$  and  $E_f$  denote the final three-momenta  $\mathbf{k}_1$ ,  $\mathbf{k}_2$ ,  $\mathbf{q}$  and the final energies  $E_{\chi_1}$ ,  $E_{\chi_2}$ , and  $E_\gamma$  of the neutralinos and the photon, respectively. The squared matrix element  $|\mathcal{M}|^2$  in (2.11) can be written as [33]

$$|\mathcal{M}|^2 = \sum_{i \leq j} T_{ij}, \quad (2.12)$$

where  $T_{ij}$  are squared amplitudes corresponding to the Feynman diagrams in Fig. 4. An average over initial spins and a sum over the spins of the outgoing neutralinos, as well as a sum over the polarizations of the outgoing pho-

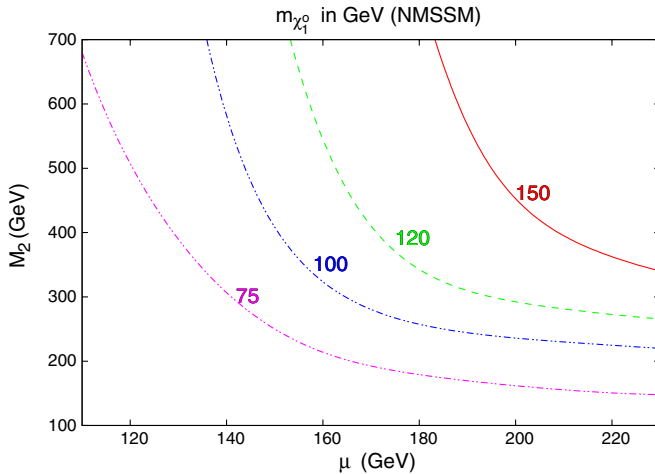


FIG. 2 (color online). Contour plots of constant lightest neutralino mass  $m_{\chi_1^0}$  in the  $\mu$ - $M_2$  plane for the NMSSM.

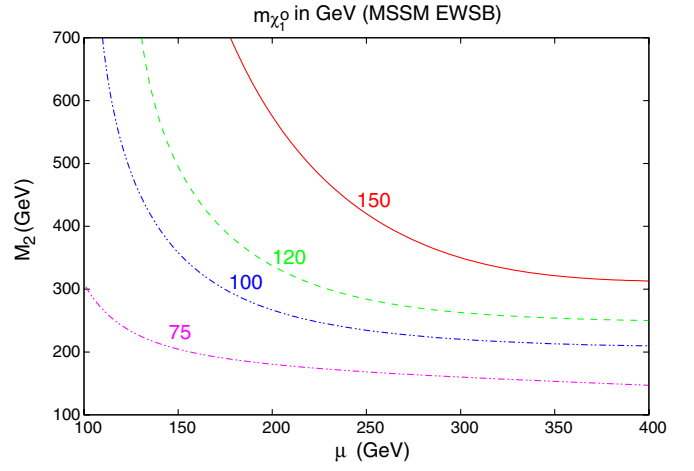


FIG. 3 (color online). Contour plots of constant lightest neutralino mass  $m_{\chi_1^0}$  in the  $\mu$ - $M_2$  plane for the MSSM.

ton, are included in  $T_{ij}$ . The phase space in (2.11) is described in [33].

### I. Numerical results

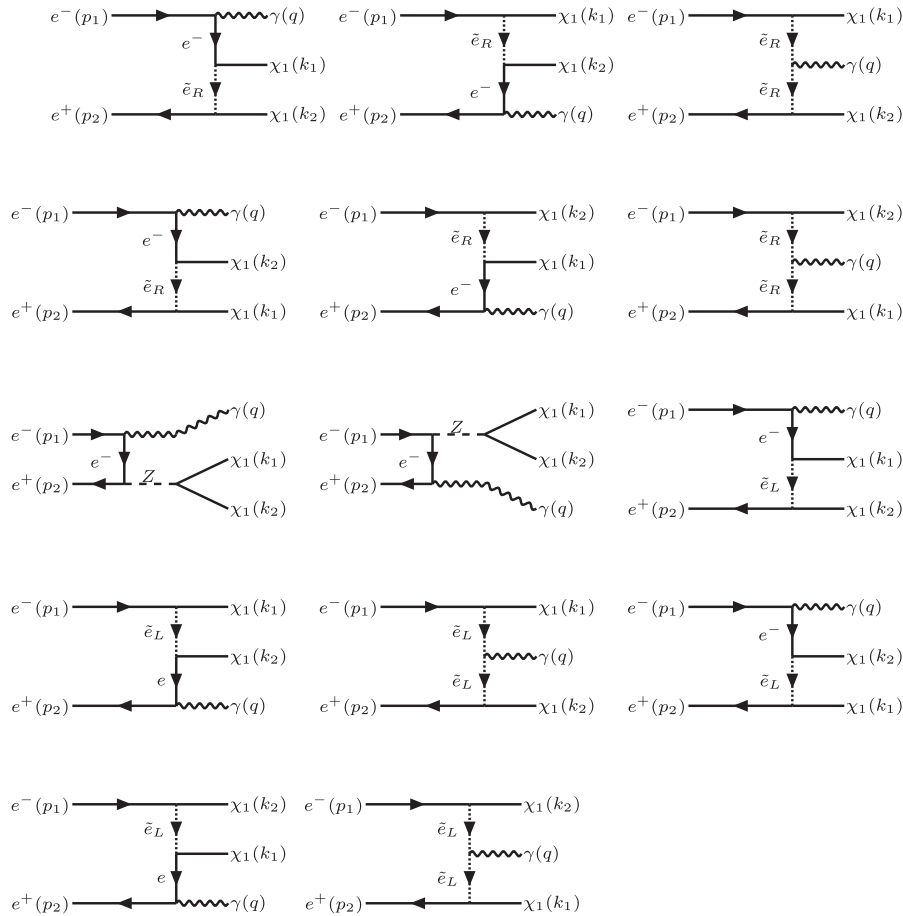
The tree-level cross section for radiative neutralino production (2.1) and the background from radiative neutrino and sneutrino production, (1.4) and (1.5), have been calculated using the program CALCHEP [54]. The tree-level cross sections have infrared and collinear divergences, which need to be regularized. To do this we define the fraction of the beam energy carried by the photon as  $x = E_\gamma/E_{\text{beam}}$ , where  $\sqrt{s} = 2E_{\text{beam}}$  is the center-of-mass energy, and  $E_\gamma$  is the energy carried away by the photon. We then impose the following cuts on  $x$ , and on the scattering angle  $\theta_\gamma$  of the photon [33,50]:

$$0.02 \leq x \leq 1 - \frac{m_{\chi_1^0}^2}{E_{\text{beam}}^2}, \quad (2.13)$$

$$-0.99 \leq \cos\theta_\gamma \leq 0.99. \quad (2.14)$$

The lower cut on  $x$  in (2.13) corresponds to a photon energy  $E_\gamma = 5$  GeV for  $\sqrt{s} = 500$  GeV. The upper cut of  $(1 - m_{\chi_1^0}^2/E_{\text{beam}}^2)$  on  $x$  corresponds to the kinematical limit of radiative neutralino production.

In order to implement the cuts on the photon energy in the calculation of the cross sections, we have taken the mass of the lightest neutralino in the NMSSM to be  $m_{\chi_1^0} = 77$  GeV for the parameter set shown in Table IV. For the MSSM, we take  $m_{\chi_1^0} = 97$  GeV from the SPS 1a scenario. Using Eq. (2.13) we get a fixed upper limit  $E_\gamma^{\text{max}} = 226$  GeV for the NMSSM and  $E_\gamma^{\text{max}} = 212$  GeV for the MSSM at  $\sqrt{s} = 500$  GeV for the photon energy. We have used exclusively these cuts for both signal and background processes. Two different mechanisms have been chosen for

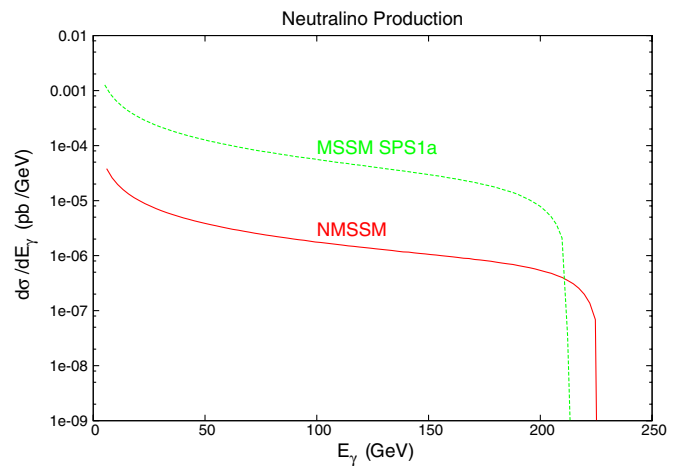

 FIG. 4. Feynman diagrams contributing to the radiative neutralino production  $e^+e^- \rightarrow \tilde{\chi}_1^0 \tilde{\chi}_1^0 \gamma$ .

the production of neutrinos in the background process (1.4), one “with upper cut” and another “without upper cut,” for obvious reasons. We note that at  $\sqrt{s} = 500$  GeV and for  $m_{\tilde{\chi}_1^0} \gtrsim 70$  GeV, this cut reduces a substantial amount of the on-shell Z boson contribution to radiative neutrino production processes.

## 2. Photon energy ( $E_\gamma$ ) distribution and total beam energy ( $\sqrt{s}$ ) dependence

Using the procedure described above, we have calculated the energy distribution of the photons from radiative neutralino production in the NMSSM and in the MSSM SPS 1a scenarios, respectively. This is shown in Fig. 5, where we compare the energy distribution of the photons in the two models. We note that the mass of the lightest neutralino is larger in the MSSM SPS 1a scenario than in the NMSSM for the set of parameters in Tables II and IV, respectively, and consequently, the upper cut for the MSSM is lower than that for the NMSSM. We also show the total beam energy  $\sqrt{s}$  dependence of the cross sections in Fig. 6 for the NMSSM and the MSSM SPS 1a, respectively. Because of a smaller value of the mass of the neutralino in the NMSSM compared to the MSSM SPS 1a, the total cross section in the NMSSM is less than that in

the MSSM SPS 1a. From the kinematical endpoint  $E_\gamma^{\max} = E_\gamma^{\max}(m_{\tilde{\chi}_1^0})$  of the energy distribution of the photon from radiative neutralino production, the neutralino mass can, in principle, be determined for  $\sqrt{s} = 500$  GeV. We note that,


 FIG. 5 (color online). Photon energy distribution  $\frac{d\sigma}{dE_\gamma}$  for the radiative neutralino production for the NMSSM (red solid line) and for the MSSM (green dashed line) at  $\sqrt{s} = 500$  GeV.

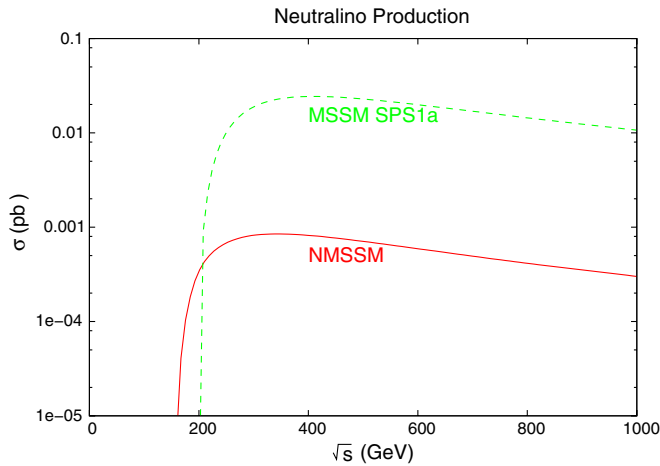


FIG. 6 (color online). Total energy  $\sqrt{s}$  dependence of the cross sections  $\sigma$  for radiative neutralino production  $e^+e^- \rightarrow \tilde{\chi}_1^0 \tilde{\chi}_1^0 \gamma$  for the NMSSM (red solid line) and for the MSSM SPS 1a scenario (green dashed line).

although the shapes of the energy distribution and the total cross section are similar in the NMSSM and MSSM, the numerical values for the NMSSM are considerably smaller as compared to the MSSM. This is primarily due to the fact that the lightest neutralino in the NMSSM has a significant singlet component, thereby reducing the cross section.

### 3. Dependence on $\mu$ and $M_2$

Since the neutralino mass matrix, and hence the lightest neutralino mass, depends on  $\mu$  and  $M_2$ , it is important to study the dependence of the radiative neutralino cross section on these parameters. In the nonminimal supersymmetric standard model,  $\mu$  ( $\equiv \lambda \langle S \rangle = \lambda x$ ) and  $M_2$  are independent parameters. We have, therefore, studied the cross section  $\sigma(e^+e^- \rightarrow \tilde{\chi}_1^0 \tilde{\chi}_1^0 \gamma)$  as a function of  $\mu$  and  $M_2$  independently. In Fig. 7 we show the  $\mu$  dependence of the total cross section for the radiative production of neutralinos for the NMSSM as well as the MSSM (EWSB). We recall that in the MSSM SPS 1a scenario these parameters are fixed. As is seen from Fig. 7, the total cross section increases with  $\mu$ . The total cross section versus  $\mu$  in Fig. 7 is plotted in the range  $\mu \in [120, 200]$  GeV in the NMSSM and in the MSSM (EWSB). Note that the parameter values are chosen so as to avoid color and charge breaking minima, absence of the Landau pole, and the phenomenological constraints on different particle masses. Furthermore, in Fig. 8, we show the  $M_2$  dependence of the total cross section for radiative neutralino production for the NMSSM and MSSM. The total cross section decreases with an increasing value of  $M_2$ . The graph of the total cross section versus  $M_2$  in Fig. 8 is plotted for the interval  $M_2 \in [300, 900]$  GeV in the NMSSM and in the MSSM (EWSB) so as to satisfy the theoretical and phenomenological constraints described above. It is clear from Fig. 8 that the radiative neutralino production cross section in the

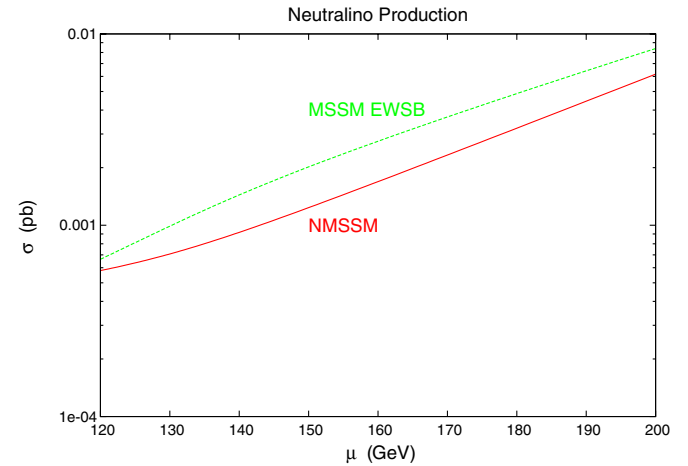


FIG. 7 (color online). Total cross section  $\sigma$  for the radiative neutralino production versus  $\mu$  for the NMSSM (red solid line) and for the MSSM in the EWSB scenario (green dashed line) at  $\sqrt{s} = 500$  GeV. For the NMSSM  $\mu \equiv \lambda \langle S \rangle = \lambda x$ .

MSSM decreases sharply as compared to that in the NMSSM.

### 4. Dependence on the selectron masses

The cross section for radiative neutralino production  $\sigma(e^+e^- \rightarrow \tilde{\chi}_1^0 \tilde{\chi}_1^0 \gamma)$  proceeds mainly via right and left selectron  $\tilde{e}_{R,L}$  exchange in the  $t$  and  $u$  channels. In the NMSSM and MSSM (EWSB), the selectron masses are independent parameters. In Figs. 9 and 10 we show the dependence of the total cross section of radiative neutralino production on the left and right selectron masses. The cross section is not very sensitive to the selectron masses for both models. Furthermore, the total neutralino production cross section is smaller in the NMSSM as compared to the

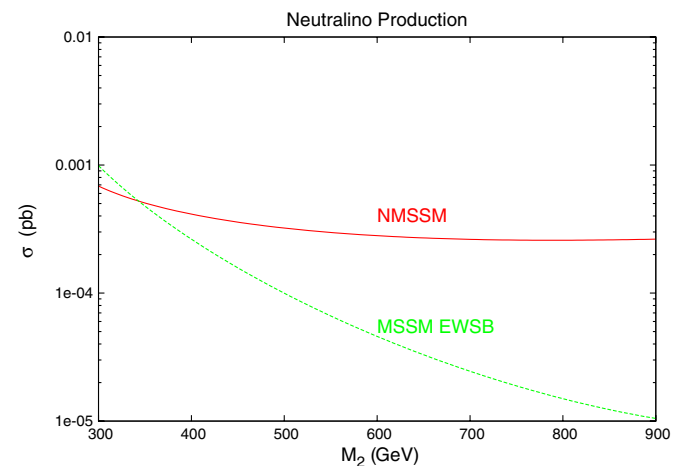


FIG. 8 (color online). Total cross section  $\sigma$  for the radiative neutralino production versus  $M_2$  for the NMSSM (red solid line) and for the MSSM in the EWSB scenario (green dashed line) at  $\sqrt{s} = 500$  GeV.

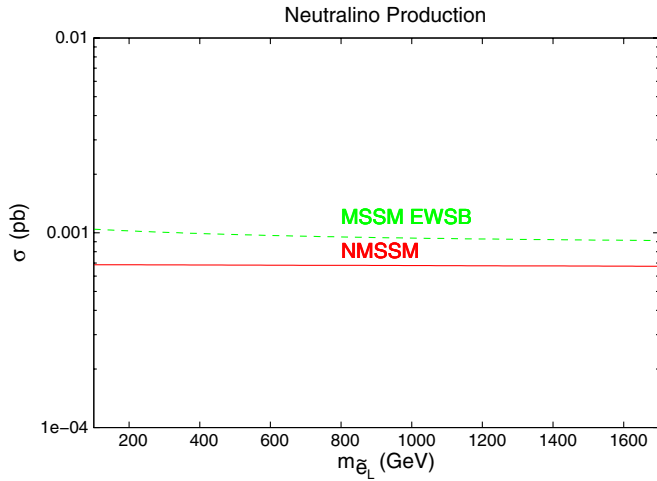


FIG. 9 (color online). Total cross section  $\sigma$  for the radiative neutralino production versus  $m_{\tilde{e}_L}$  for the NMSSM (red solid line) and for the MSSM in the EWSB scenario (green dashed line) at  $\sqrt{s} = 500$  GeV.

MSSM (EWSB) as a function of left as well as right selectron masses.

### 5. Photon energy ( $E_\gamma$ ) distribution for the radiative production of the second lightest neutralino

As discussed above, the cross section for the production of the lightest neutralino in the NMSSM is rather small compared with the corresponding cross section for the lightest neutralino in the MSSM. It may, therefore, be useful to consider the radiative production of the second lightest neutralino in the NMSSM. For the parameter set of Table IV the composition of the second lightest neutralino in the NMSSM is given by

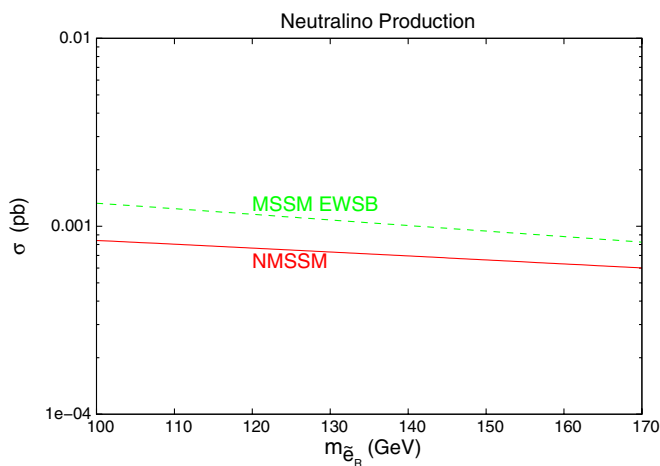


FIG. 10 (color online). Total cross section  $\sigma$  for the radiative neutralino production versus  $m_{\tilde{e}_R}$  for the NMSSM (red solid line) and for the MSSM in the EWSB scenario (green dashed line) at  $\sqrt{s} = 500$  GeV.

$$N'_{2j} = (-0.085, 0.1, 0.69, 0.68, 0.19). \quad (2.15)$$

We have calculated the photon energy distribution for the radiative production of the second lightest neutralino in the NMSSM for the set of parameters shown in Table IV. This is shown in Fig. 11. For comparison we have also shown the photon energy distribution for the radiative production of the lightest neutralino in the MSSM for the SPS 1a scenario. We see that the cross section for the production of the second lightest neutralino in the NMSSM is much smaller than the cross section for the lightest neutralino in the MSSM.

## III. BACKGROUND PROCESSES

### A. The neutrino background

The major background to the radiative neutralino production (2.1) comes from the SM radiative neutrino production process [40,47,56–58]

$$e^+ + e^- \rightarrow \nu_\ell + \bar{\nu}_\ell + \gamma, \quad \ell = e, \mu, \tau. \quad (3.1)$$

In this process  $\nu_e$  are produced via  $t$ -channel  $W$  boson exchange, and  $\nu_{e,\mu,\tau}$  via  $s$ -channel  $Z$  boson exchange. We show the corresponding Feynman diagrams in Fig. 12.

The background photon energy distribution  $\frac{d\sigma}{dE_\gamma}$  and  $\sqrt{s}$  dependence of the cross section  $\sigma$  for radiative neutrino production  $e^+e^- \rightarrow \nu\bar{\nu}\gamma$  is the same for both the NMSSM and the MSSM. As shown in Fig. 13 the photon energy distribution from the radiative neutrino production peaks at  $E_\gamma = (s - m_Z^2)/(2\sqrt{s}) \approx 242$  GeV because of the radiative  $Z$  production ( $\sqrt{s} > m_Z$ ). This photon background from radiative neutrino production can be reduced by imposing an upper cut on the photon energy  $x^{\max} = E_\gamma^{\max}/E_{\text{beam}} = 1 - m_{\chi_1^0}^2/E_{\text{beam}}^2$  [see Eq. (2.13)], which is

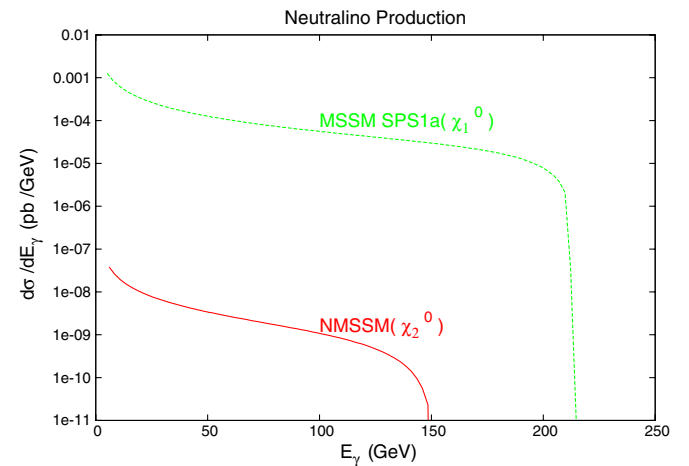
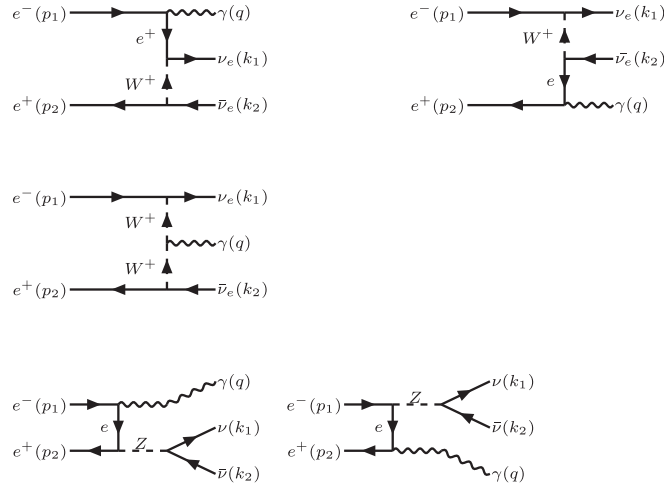


FIG. 11 (color online). Photon energy distribution  $\frac{d\sigma}{dE_\gamma}$  for the radiative production of the second lightest neutralino ( $\chi_2^0$ ) for the NMSSM (red solid line) and for the lightest neutralino ( $\chi_1^0$ ) for the MSSM (green dashed line) at  $\sqrt{s} = 500$  GeV.

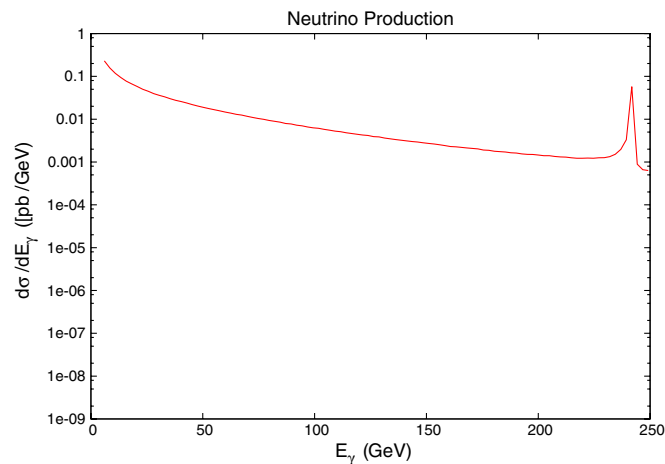

 FIG. 12. Feynman diagrams contributing to the radiative neutrino process  $e^+e^- \rightarrow \nu\bar{\nu}\gamma$ .

the kinematical endpoint  $E_\gamma^{\max} \approx 226$  GeV of the energy distribution of the photon from radiative neutralino production,

$$m_{\chi_1^0}^2 = \frac{1}{4}(s - 2\sqrt{s}E_\gamma^{\max}). \quad (3.2)$$

In order to achieve this, one would have to separate the signal and background processes. This would be possible if the neutralino is heavy enough, such that the endpoint is removed from the  $Z^0$  peak of the background distribution.

In Fig. 14 we show the  $\sqrt{s}$  dependence of the total radiative neutrino cross section. Without the upper cut on the photon energy  $\chi^{\max}$ , the background cross section from radiative neutrino production  $e^+e^- \rightarrow \nu\bar{\nu}\gamma$  (green points in Fig. 14) is much larger than the corresponding cross section with the cut (solid red line). However, when we impose the cut, the signal cross section from radiative neutralino production is only about 1 order of magnitude smaller than the background in the case of the MSSM, but


 FIG. 13 (color online). The photon energy distribution  $\frac{d\sigma}{dE_\gamma}$  for the radiative neutrino process  $e^+e^- \rightarrow \nu\bar{\nu}\gamma$  at  $\sqrt{s} = 500$  GeV.

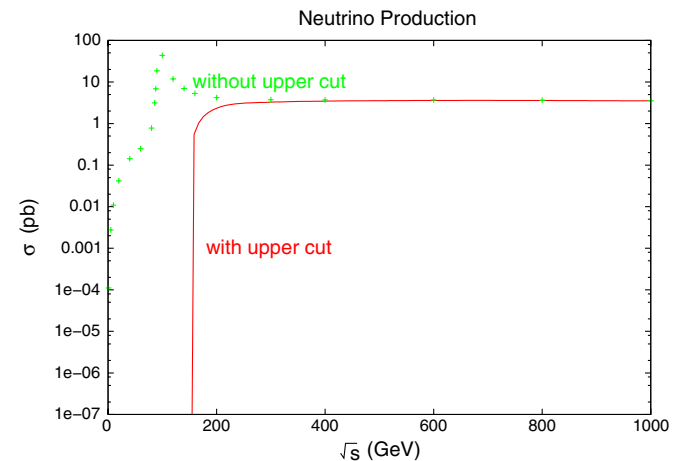
is nearly 3 orders of magnitude smaller than the background in the case of the NMSSM.

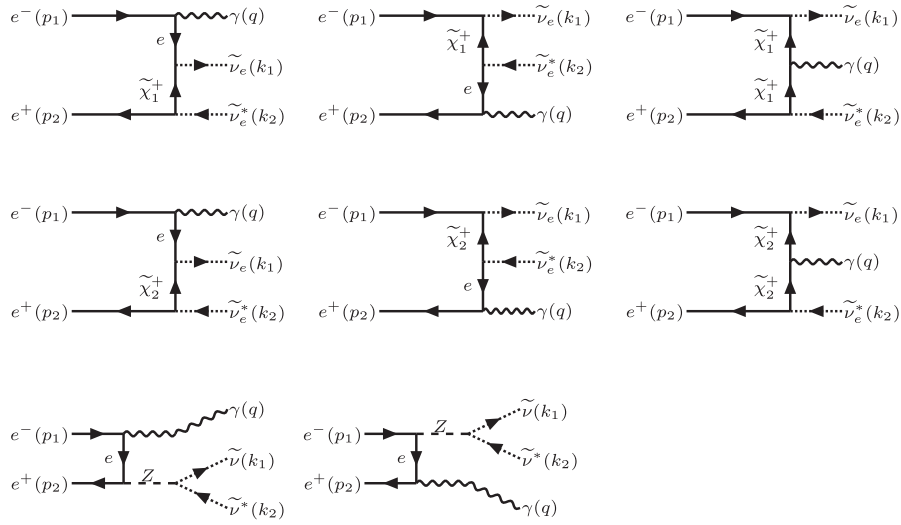
### B. The supersymmetric background

Apart from the SM background coming from (3.1), the radiative neutralino production (2.1) has a background coming from the supersymmetric sneutrino production process [40,59]

$$e^+ + e^- \rightarrow \tilde{\nu}_\ell + \tilde{\nu}_\ell^* + \gamma, \quad \ell = e, \mu, \tau. \quad (3.3)$$

The lowest order Feynman diagrams contributing to the process (3.3) are shown in Fig. 15. This process receives  $t$ -channel contributions via virtual charginos for  $\tilde{\nu}_\ell \tilde{\nu}_\ell^*$  production, as well as  $s$ -channel contributions from  $Z$  boson exchange for  $\tilde{\nu}_{e,\mu,\tau} \tilde{\nu}_{e,\mu,\tau}^*$  production. In Fig. 16, we show the photon energy distribution  $\frac{d\sigma}{dE_\gamma}$  for radiative sneutrino

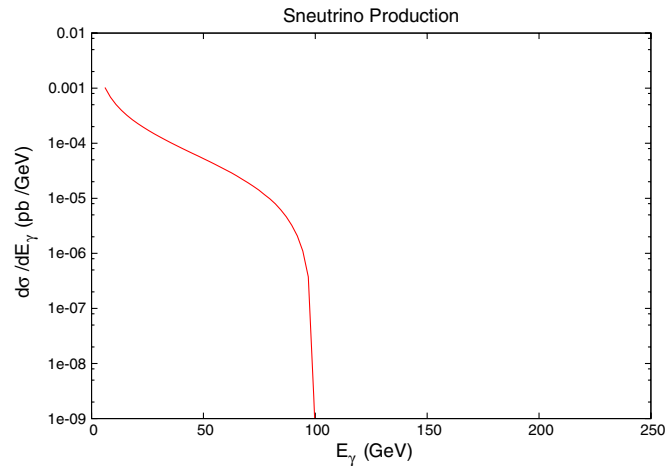

 FIG. 14 (color online). The total energy  $\sqrt{s}$  dependence of the radiative neutrino cross section  $\sigma(e^+e^- \rightarrow \nu\bar{\nu}\gamma)$  with an upper cut (red line) on the photon energy  $E_\gamma$ , and of the radiative neutrino cross section without an upper cut (green points) on the photon energy  $E_\gamma$ ; see Eq. (2.13).


 FIG. 15. Feynman diagrams contributing to the radiative sneutrino production process  $e^+e^- \rightarrow \tilde{\nu}\tilde{\nu}^*\gamma$ .

production  $e^+e^- \rightarrow \tilde{\nu}\tilde{\nu}^*\gamma$  at  $\sqrt{s} = 500$  GeV. The total cross section for the radiative sneutrino production is shown in Fig. 17.

Radiative sneutrino production (3.3) can be a major supersymmetric background to neutralino production (2.1) if sneutrinos decay mainly invisibly, e.g. via  $\tilde{\nu} \rightarrow \tilde{\chi}_1^0 \nu$ . This leads to the so-called ‘‘virtual LSP’’ scenario [40]. However, if kinematically allowed, other visible decay channels like  $\tilde{\nu} \rightarrow \tilde{\chi}_1^\pm \ell^\mp$  reduce the background rate from radiative sneutrino production. For example, in the SPS 1a scenario [51,60] of the MSSM we have  $\text{BR}(\tilde{\nu}_e \rightarrow \tilde{\chi}_1^0 \nu_e) = 85\%$ .

Furthermore, neutralino production  $e^+e^- \rightarrow \tilde{\chi}_1^0 \tilde{\chi}_2^0$  followed by subsequent radiative neutralino decay [61]  $\tilde{\chi}_2^0 \rightarrow \tilde{\chi}_1^0 \gamma$  is also a potential background. However, significant branching ratios  $\text{BR}(\tilde{\chi}_2^0 \rightarrow \tilde{\chi}_1^0 \gamma) > 10\%$  are only obtained for small values of  $\tan\beta < 5$  and/or  $M_1 \sim M_2$  [41,62,63].


 FIG. 16 (color online). The photon energy distribution  $\frac{d\sigma}{dE_\gamma}$  for the radiative sneutrino production  $e^+e^- \rightarrow \tilde{\nu}\tilde{\nu}^*\gamma$  at  $\sqrt{s} = 500$  GeV.

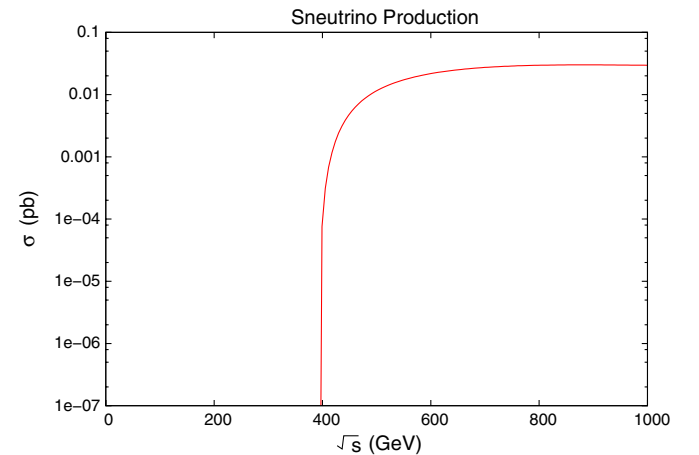
Thus, we neglect this background, detailed discussions of which can be found in Refs. [62–64].

### C. Theoretical significance

We now consider the question as to whether an excess of photons from radiative neutralino production can be measured over the SM background photons coming from radiative neutrino production. To quantify the excess of photons from the signal over the SM background photons for a given integrated luminosity  $\mathcal{L}$ , we consider the theoretical significance [50]

$$S = \frac{N_S}{\sqrt{N_S + N_B}} = \frac{\sigma}{\sqrt{\sigma + \sigma_B}} \sqrt{\mathcal{L}}, \quad (3.4)$$

where  $N_S = \sigma \mathcal{L}$  is the number of signal photons, and  $N_B = \sigma_B \mathcal{L}$  is the number of photons from the SM background of the radiative neutrino production process.


 FIG. 17 (color online). Total energy  $\sqrt{s}$  dependence of the radiative sneutrino production cross section  $\sigma(e^+e^- \rightarrow \tilde{\nu}\tilde{\nu}^*\gamma)$ .

The processes  $e^+e^- \rightarrow \tilde{\chi}_1^0 \tilde{\chi}_1^0 \gamma$  and  $e^+e^- \rightarrow \nu \bar{\nu} \gamma$  depend significantly on the beam energy only near threshold in most of the parameter space for  $\sqrt{s} = 500$  GeV and  $\mathcal{L} = 5 \times 10^5 \text{ pb}^{-1}$ . In Fig. 18, we show the  $\mu$  dependence of the theoretical significance  $S$  for the NMSSM. For this plot we have chosen  $A_\lambda = 0$ , and varied the parameter  $\mu$  in the interval  $\mu \in [110, 220]$  GeV. All other parameters for the NMSSM are chosen as in Table IV. For comparison we have also shown in Fig. 18 the theoretical significance  $S$  for the MSSM with parameters as in Table III for the EWSB model. We note that in the NMSSM for  $\mu < 110$  GeV, and with other parameters as described above, the Landau pole develops below the GUT scale, and the lightest chargino and the lightest neutralino masses are below the experimental lower bounds. On the other hand, for  $\mu > 220$  GeV, the NMSSM develops unphysical global minima. We note from this analysis that the significance of  $S \approx 4$  can be attained for  $\mu \approx 220$  GeV.

We have also studied the behavior of the theoretical significance as a function of the  $SU(2)_L$  gaugino mass  $M_2$ . In Fig. 19, we show the  $M_2$  dependence of the theoretical significance  $S$  for the NMSSM and the MSSM in the interval  $M_2 \in [300, 900]$  GeV. As in the study of the  $\mu$  dependence, for the NMSSM we have chosen  $A_\lambda = 0$ , and all other parameters as in Table IV. Furthermore, for the NMSSM the interval for  $M_2$  is chosen in order to satisfy the theoretical and experimental constraints. For  $M_2 < 300$  GeV, the Landau pole for the NMSSM develops below the GUT scale. On the other hand, for values of  $M_2 > 900$ , there is a sfermion with negative mass squared in the spectrum of the NMSSM. We note from Figs. 18 and 19 that higher values of  $\mu$  and lower values of  $M_2$  are favored for achieving higher values of the significance  $S$ . A theoretical significance of  $S = 1$  would mean that the signal can be measured at a 68% confidence level. On the other

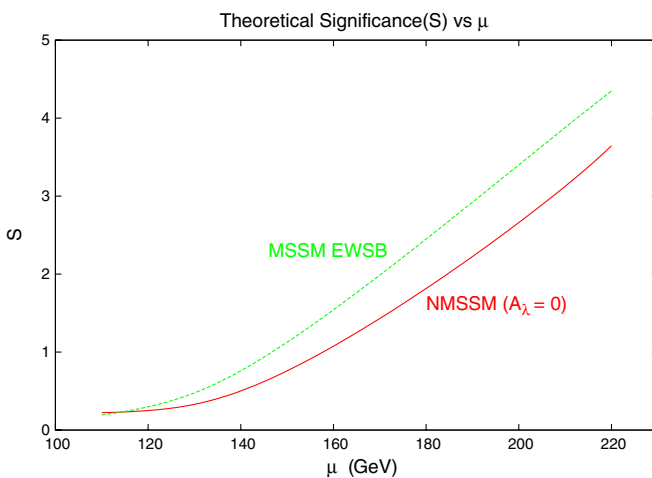


FIG. 18 (color online). Theoretical significance  $S = \frac{\sigma}{\sqrt{\sigma^+ \sigma_B}} \times \sqrt{\mathcal{L}}$  for the radiative neutralino production versus  $\mu$  for the NMSSM (red solid line) and for the MSSM in the EWSB scenario (green dashed line). The value of  $\sqrt{s} = 500$  GeV.

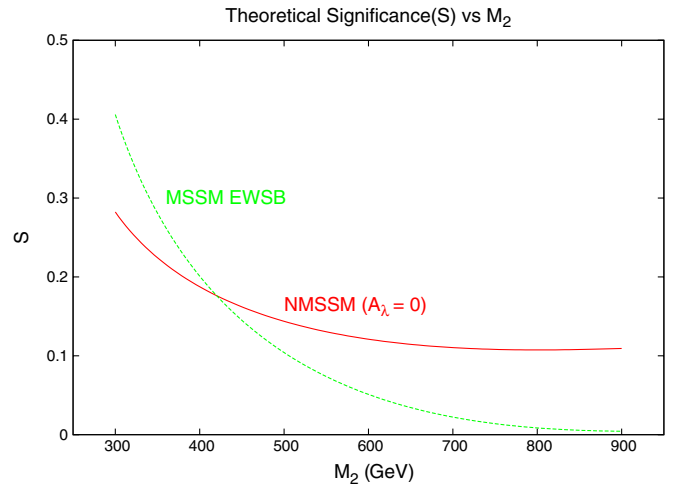


FIG. 19 (color online). Theoretical significance  $S = \frac{\sigma}{\sqrt{\sigma^+ \sigma_B}} \times \sqrt{\mathcal{L}}$  for the radiative neutralino production versus  $M_2$  for the NMSSM (red solid line) and for the MSSM in the EWSB scenario (green dashed line). The value of  $\sqrt{s} = 500$  GeV.

hand, a significance of 5 is required for the detection of the signal. We note that a signal significance of about 4 can be achieved for the NMSSM for values of  $\mu \approx 220$  GeV. Besides the theoretical significance, one must also consider the signal to background ratio  $N_S/N_B$  in order to judge the reliability of the analysis. It will be necessary to do a detailed Monte Carlo analysis to predict the significance. However, this is beyond the scope of the present work.

#### IV. SUMMARY AND CONCLUSIONS

The nonminimal supersymmetric standard model is an attractive low energy supersymmetric model which solves the  $\mu$  problem of the minimal supersymmetric standard model. We have carried out a detailed analysis of the radiative neutralino production  $e^+e^- \rightarrow \tilde{\chi}_1^0 \tilde{\chi}_1^0 \gamma$  in the NMSSM for the International Linear Collider energies and compared it with the corresponding results in the MSSM. This process has a signature of a high energy photon and missing energy. We have obtained a typical set of parameter values for the NMSSM by imposing theoretical and experimental constraints on the parameter space of the NMSSM. For the set of parameter values that we obtain in this manner, the lightest neutralino in the NMSSM has a significant admixture of the fermionic component of the singlet chiral superfield  $S$ . Using this parameter set, we have studied in detail the radiative neutralino production cross section in the NMSSM for the ILC energies with unpolarized  $e^+$  and  $e^-$  beams. For comparison, we have used the SPS 1a benchmark scenario for the MSSM. We have also calculated the background to this process from the SM process  $e^+e^- \rightarrow \nu \bar{\nu} \gamma$ , as well as the background from the supersymmetric process  $e^+e^- \rightarrow \tilde{\nu} \tilde{\nu}^* \gamma$ . All these processes have a signature of a highly energetic photon with missing energy. The photon energy

distribution  $d\sigma/dE_\gamma$ , and the total cross section as a function of the total energy have been calculated for the NMSSM and for the MSSM SPS 1a scenario at  $\sqrt{s} = 500$  GeV using CALCHEP. Because of the admixture of a singlet in the lightest neutralino, the cross section as a function of energy for the radiative neutralino production is much lower in the NMSSM than in the MSSM. We have also studied the dependence of the cross section for radiative neutralino production on the  $SU(2)_L$  gaugino mass parameter  $M_2$  and the Higgs(ino) mass parameter  $\mu$ , as well as its dependence on the selectron ( $\tilde{e}_R, \tilde{e}_L$ ) masses in the NMSSM, and compared it with the corresponding results in the MSSM. In order to quantify whether an excess of signal photons,  $N_S$ , can be measured over the background photons,  $N_B$ , from radiative neutrino production, we have analyzed the theoretical statistical significance  $S = N_S/\sqrt{N_S + N_B}$ , and studied its dependence on  $M_2$  and  $\mu$ , the parameters that enter the neutralino mass

matrix. The theoretical significance increases with the parameter  $\mu$  for the NMSSM as well as the MSSM, whereas it decreases as a function of  $M_2$ . The decrease is especially sharp in the case of the minimal supersymmetric standard model. It may be interesting to study whether the signal for radiative neutralino production in the NMSSM can be enhanced by using polarized beams [65].

## ACKNOWLEDGMENTS

P.N.P. would like to thank The Institute of Mathematical Sciences, Chennai, where this work was started, for its hospitality. He would also like to thank the Abdus Salam ICTP, where this work was completed, for its hospitality. The work of P.N.P. is supported by the Board of Nuclear Sciences, Department of Atomic Energy, India under Project No. 2007/37/34/BRNS/1970.

- 
- [1] J. Wess and J. Bagger, *Supersymmetry and Supergravity* (Princeton University Press, Princeton, NJ, 1992), p. 259.
- [2] G. 't Hooft, in *Recent Developments in Gauge Theories*, NATO Advanced Study Institutes, Ser. B, Vol. 59 (Plenum, New York, 1980), p. 438; E. Witten, Nucl. Phys. **B188**, 513 (1981); R. K. Kaul, Phys. Lett. **109B**, 19 (1982); R. K. Kaul and P. Majumdar, Nucl. Phys. **B199**, 36 (1982); R. K. Kaul, Pramana **19**, 183 (1982).
- [3] H. P. Nilles, Phys. Rep. **110**, 1 (1984).
- [4] M. Drees, R. Godbole, and P. Roy, *Theory and Phenomenology of Sparticles: An Account of Four-dimensional  $N = 1$  Supersymmetry in High Energy Physics* (World Scientific, Hackensack, NJ, 2004), p. 555.
- [5] J. A. Aguilar-Saavedra *et al.* (ECFA/DESY LC Physics Working Group), arXiv:hep-ph/0106315.
- [6] T. Abe *et al.* (American Linear Collider Working Group), arXiv:hep-ex/0106055.
- [7] K. Abe *et al.* (ACFA Linear Collider Working Group), arXiv:hep-ph/0109166.
- [8] G. Weiglein *et al.* (LHC/LC Study Group), Phys. Rep. **426**, 47 (2006).
- [9] J. A. Aguilar-Saavedra *et al.*, Eur. Phys. J. C **46**, 43 (2006).
- [10] G. A. Moortgat-Pick *et al.*, arXiv:hep-ph/0507011.
- [11] P. Fayet, Nucl. Phys. **B90**, 104 (1975); H. P. Nilles, M. Srednicki, and D. Wyler, Phys. Lett. **120B**, 346 (1983); J. P. Derendinger and C. A. Savoy, Nucl. Phys. **B237**, 307 (1984).
- [12] J. R. Ellis, J. F. Gunion, H. E. Haber, L. Roszkowski, and F. Zwirner, Phys. Rev. D **39**, 844 (1989).
- [13] M. Drees, Int. J. Mod. Phys. A **4**, 3635 (1989).
- [14] P. N. Pandita, Phys. Lett. B **318**, 338 (1993); P. N. Pandita, Z. Phys. C **59**, 575 (1993); U. Ellwanger, Phys. Lett. B **303**, 271 (1993); U. Ellwanger, M. Rausch de Traubenberg, and C. A. Savoy, Phys. Lett. B **315**, 331 (1993); S. F. King and P. L. White, Phys. Rev. D **53**, 4049 (1996).
- [15] B. Ananthanarayan and P. N. Pandita, Int. J. Mod. Phys. A **12**, 2321 (1997).
- [16] B. Ananthanarayan and P. N. Pandita, Phys. Lett. B **371**, 245 (1996).
- [17] B. Ananthanarayan and P. N. Pandita, Phys. Lett. B **353**, 70 (1995).
- [18] M. Chemtob and P. N. Pandita, Phys. Rev. D **73**, 055012 (2006).
- [19] M. Chemtob and P. N. Pandita, Phys. Rev. D **76**, 095019 (2007).
- [20] R. Dermisek and J. F. Gunion, Phys. Rev. Lett. **95**, 041801 (2005).
- [21] U. Ellwanger, J. F. Gunion, and C. Hugonie, J. High Energy Phys. 07 (2005) 041.
- [22] G. A. Moortgat-Pick, S. Hesselbach, F. Franke, and H. Fraas, arXiv:hep-ph/0508313.
- [23] J. F. Gunion, D. Hooper, and B. McElrath, Phys. Rev. D **73**, 015011 (2006).
- [24] P. N. Pandita, Phys. Rev. D **50**, 571 (1994).
- [25] P. N. Pandita, Z. Phys. C **63**, 659 (1994).
- [26] S. Y. Choi, D. J. Miller, and P. M. Zerwas, Nucl. Phys. **B711**, 83 (2005).
- [27] H. Goldberg, Phys. Rev. Lett. **50**, 1419 (1983).
- [28] J. R. Ellis, J. S. Hagelin, D. V. Nanopoulos, K. A. Olive, and M. Srednicki, Nucl. Phys. **B238**, 453 (1984).
- [29] A. Bartl, H. Fraas, and W. Majerotto, Nucl. Phys. **B278**, 1 (1986).
- [30] J. R. Ellis, J. M. Frere, J. S. Hagelin, G. L. Kane, and S. T. Petcov, Phys. Lett. **132B**, 436 (1983); E. Reya, Phys. Lett. **133B**, 245 (1983); P. Chiappetta, J. Soffer, P. Taxil, F. M. Renard, and P. Sorba, Nucl. Phys. **B262**, 495 (1985); **B279**, 824(E) (1987).
- [31] P. Fayet, Phys. Lett. **117B**, 460 (1982).

- [32] J. R. Ellis and J. S. Hagelin, *Phys. Lett.* **122B**, 303 (1983).
- [33] K. Grassie and P. N. Pandita, *Phys. Rev. D* **30**, 22 (1984).
- [34] T. Kobayashi and M. Kuroda, *Phys. Lett.* **139B**, 208 (1984).
- [35] J. D. Ware and M. E. Machacek, *Phys. Lett.* **142B**, 300 (1984).
- [36] L. Bento, J. C. Romao, and A. Barroso, *Phys. Rev. D* **33**, 1488 (1986).
- [37] M. Chen, C. Dionisi, M. Martinez, and X. Tata, *Phys. Rep.* **159**, 201 (1988).
- [38] T. Kon, *Prog. Theor. Phys.* **79**, 1006 (1988).
- [39] S. Y. Choi, J. S. Shim, H. S. Song, J. Song, and C. Yu, *Phys. Rev. D* **60**, 013007 (1999).
- [40] A. Datta, A. Datta, and S. Raychaudhuri, *Eur. Phys. J. C* **1**, 375 (1998); A. Datta, A. Datta, and S. Raychaudhuri, *Phys. Lett. B* **349**, 113 (1995).
- [41] S. Ambrosanio, B. Mele, G. Montagna, O. Nicrosini, and F. Piccinini, *Nucl. Phys.* **B478**, 46 (1996).
- [42] A. Heister *et al.* (ALEPH Collaboration), *Eur. Phys. J. C* **28**, 1 (2003).
- [43] J. Abdallah *et al.* (DELPHI Collaboration), *Eur. Phys. J. C* **38**, 395 (2005).
- [44] P. Achard *et al.* (L3 Collaboration), *Phys. Lett. B* **587**, 16 (2004).
- [45] G. Abbiendi *et al.* (OPAL Collaboration), *Eur. Phys. J. C* **26**, 479 (2003).
- [46] G. Abbiendi *et al.* (OPAL Collaboration), *Eur. Phys. J. C* **18**, 253 (2000).
- [47] K. J. F. Gaemers, R. Gastmans, and F. M. Renard, *Phys. Rev. D* **19**, 1605 (1979).
- [48] D. Choudhury, H. K. Dreiner, P. Richardson, and S. Sarkar, *Phys. Rev. D* **61**, 095009 (2000); A. Dedes, H. K. Dreiner, and P. Richardson, *Phys. Rev. D* **65**, 015001 (2001); H. K. Dreiner, C. Hanhart, U. Langenfeld, and D. R. Phillips, *Phys. Rev. D* **68**, 055004 (2003).
- [49] M. Gataullin (LEP Collaboration), *Eur. Phys. J. C* **33**, S791 (2004).
- [50] H. K. Dreiner, O. Kittel, and U. Langenfeld, *Phys. Rev. D* **74**, 115010 (2006).
- [51] B. C. Allanach *et al.*, *Eur. Phys. J. C* **25**, 113 (2002).
- [52] H. E. Haber and G. L. Kane, *Phys. Rep.* **117**, 75 (1985).
- [53] A. Bartl, H. Fraas, W. Majerotto, and N. Oshimo, *Phys. Rev. D* **40**, 1594 (1989).
- [54] A. Pukhov, arXiv:hep-ph/0412191.
- [55] S. Eidelman *et al.* (Particle Data Group), *Phys. Lett. B* **592**, 1 (2004).
- [56] F. A. Berends, G. J. H. Burgers, C. Mana, M. Martinez, and W. L. van Neerven, *Nucl. Phys.* **B301**, 583 (1988).
- [57] F. Boudjema *et al.*, arXiv:hep-ph/9601224.
- [58] G. Montagna, M. Moretti, O. Nicrosini, and F. Piccinini, *Nucl. Phys.* **B541**, 31 (1999).
- [59] F. Franke and H. Fraas, *Phys. Rev. D* **49**, 3126 (1994).
- [60] N. Ghodbane and H. U. Martyn, arXiv:hep-ph/0201233.
- [61] H. E. Haber and D. Wyler, *Nucl. Phys.* **B323**, 267 (1989).
- [62] S. Ambrosanio and B. Mele, *Phys. Rev. D* **53**, 2541 (1996).
- [63] S. Ambrosanio and B. Mele, *Phys. Rev. D* **55**, 1399 (1997); **56**, 3157(E) (1997).
- [64] H. Baer and T. Krupovnickas, *J. High Energy Phys.* 09 (2002) 038.
- [65] R. Basu, P. N. Pandita, and Chandradew Sharma (unpublished).